Deep–Sea Research I 225 (2025) 104593

Contents lists available at ScienceDirect

Deep-Sea Research Part I

journal homepage: www.elsevier.com/locate/dsri

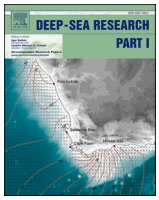

Satellite-detected sea surface chlorophyll-a penetrating fronts off the south coast of Java Island

Tengfei Xu [a,b,c], Dingqi Wang [a,b,c], Qinsheng Wei [a,b,c], Shujiang Li [a,b,c], R.D. Susanto [d,e], Guanlin Wang [a,b,c], Fei Teng [a,b,c], T. Agustiadi [f], M. Trenggono [g], Priyadi Dwi Santoso [h], Zexun Wei [a,b,c,*]

[a] Key Laboratory of Marine Science and Numerical Modeling, First Institute of Oceanography, Ministry of Natural Resources of China, Qingdao, China
[b] Laboratory for Regional Oceanography and Numerical Modeling, Qingdao Marine Science and Technology Center, Qingdao, China
[c] Shandong Key Laboratory of Marine Science and Numerical Modeling, Qingdao, China
[d] Department of Atmospheric and Oceanic Science, University of Maryland, College Park, MD, USA
[e] Faculty of Earth Sciences and Technology, Bandung Institute of Technology, Bandung, Indonesia
[f] Research Center for Oceanography, National Research and Innovation Agency, Jakarta, Indonesia
[g] Department of Marine Science, Faculty of Fisheries and Marine Science, Jenderal Soedirman University, Purwokerto, Indonesia
[h] Research Center for Deep Sea, National Research and Innovation Agency, Jakarta, Indonesia

ARTICLE INFO

Keywords:
Java upwelling
Penetrating front
Sea surface chlorophyll-a (SSC)
Mesoscale eddy
Interannual variability

ABSTRACT

In this study, we report the phenomenon of sea surface chlorophyll-a (SSC) penetrating front south of Java Island based on satellite observations. The SSC penetrating front occurs frequently (~17 times per month) during the upwelling season (June to November) and can also be observed (~4 times per month) during the non-upwelling season (December to May). The offshore distance of the SSC penetrating front can reach up to 500 km and 350 km in the upwelling and non-upwelling seasons, respectively. Eddy-related advection along the eddy edges plays an important role in maintaining the SSC penetrating front by transporting nutrient-rich waters from the Java coast. The interannual variability of the SSC penetrating front is closely associated with the ENSO and IOD events, which tend to induce anomalous upwelling and enhanced mesoscale eddy activity, thereby leading to more frequent occurrences of the SSC penetrating fronts south of Java Island.

1. Introduction

The sea surface chlorophyll-a (SSC) and its variability are of great interest, as they can be used as helpful indicators for marine primary production in the upper layer (Carr et al., 2006; Taboada et al., 2019). An application of such an approach is along the southern coast of Java Island, which is known as one of the most productive fishing grounds for tuna (Syamsuddin et al., 2016; Wirasatriya et al., 2020). The cold and nutrient-rich waters are entrained into the upper layer by upwelling along the South Java coast, resulting in an increase in phytoplankton biomass to feed higher-trophic-level organisms such as fishes (Wei et al., 2012; Lumban-Gaol et al., 2015). Consequently, the duration of the abundant season of the fisheries production generally coincides with that of the monsoon-driven coastal upwelling (Hood et al., 2017; Lahlali et al., 2018). The phytoplankton biomass increase along the south coast of Java could be well detected by high SSC concentration at intraseasonal, seasonal and interannual timescales (Iskandar et al., 2010; Kong et al., 2019; Siswanto et al., 2020; Setiawan et al., 2019; Susanto et al., 2006; Wirasatriya et al., 2020; Xu et al., 2018, 2021).

Based on satellite-derived SSC data, Yuan et al. (2005) reported a phenomenon of cross-shelf penetrating front off the Zhejiang-Fujian (Min-Zhe) coast, China. The mechanisms of the cross-shelf penetrating front are explained by wind-driven cross-shelf jet (He et al., 2010; Yuan et al., 2005, 2010), non-uniform tidal mixing induced baroclinicity and relief (Wu, 2015), frontal instability (Yuan et al., 2010), and wind-induced fluctuations and the Taiwan Warm Current (TWC) offshore meanders (Ren et al., 2015; Xuan et al., 2017). Ye et al. (2022) further examined the evolution and dynamics of the cross-shelf penetrating front off the Min-Zhe coast, suggesting that the different factors are dominant during the development, maturation, and decay stages of the penetrating front. The significance of penetrating fronts lies in two aspects. Firstly, they play an important roles in cross-shelf transport of

* Corresponding author. First Institute of Oceanography, Ministry of Natural Resources of China, Qingdao, China.
E-mail address: weizx@fio.org.cn (Z. Wei).

https://doi.org/10.1016/j.dsr.2025.104593
Received 17 April 2025; Received in revised form 30 August 2025; Accepted 17 September 2025
Available online 18 September 2025

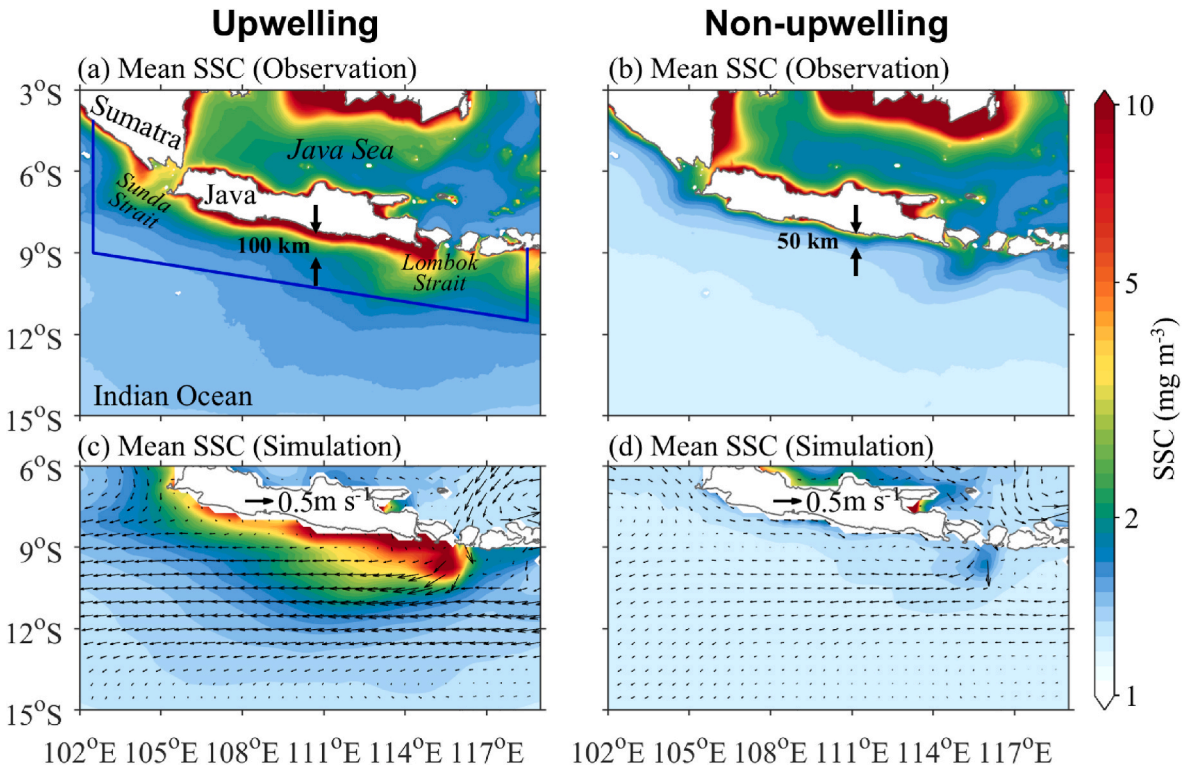

Fig. 1. Mean sea surface chlorophyll-a (SSC, unit: mg m^{-3}) during (a) upwelling (June to November) and (b) non-upwelling (December to May) periods in satellite observation; (c) and (d) are the same as (a) and (b), but from the Global Ocean Biogeochemistry Hindcast (GOBH) dataset.

coastal nutrient-rich waters and sediments (Li et al., 2003; Du et al., 2022); secondly, they exhibit intermittent signatures, instead of the previously understood relatively stable coastal fronts, and thus are more active at intraseasonal frequency band (Hickox et al., 2000; Ye et al., 2022).

Recently, the intraseasonal SSC signals along the south coast of Java have been identified using high-resolution satellite observations (Xu et al., 2021). Among these intraseasonal SSC signals, some are associated with the propagation of upwelling Kelvin waves and active mesoscale eddies (Xu et al., 2021; Yang et al., 2019). Furthermore, Malan et al. (2020) suggested an eddy-driven cross-shelf transport in the East Australian Current separation zone. Since there are active mesoscale eddies in the southeastern tropical Indian Ocean off Java Island (Yang et al., 2015; Azis Ismail et al., 2021; Wang et al., 2021; Li et al., 2022), such cross-shelf transport of nutrient-rich waters is very likely to occur from the Java coastal upwelling region to the open ocean. This process may consequently induce the formation of a SSC penetrating front. In this study, we will show the SSC penetrating fronts off the south coast of Java, and we will also discuss their variability and possible driving factors.

2. Data and methods

2.1. Data description

The SSC data were obtained from the merged product (Product ID: OCEANCOLOUR_GLO_CHL_L4_REP_OBSERVATIONS_009_082), and provided by the Copernicus Marine Environment Monitoring Service (CMEMS) (Garnesson et al., 2019). The dataset is daily, with a spatial resolution of 4 km, and is available from September 4, 1997 to the present.

The sea surface height (SSH) and sea surface geostrophic currents data are also provided by CMEMS (Product ID: SEALEVEL_GLO_PHY_L4_MY_008_047). The dataset is daily, with a spatial resolution of 0.25° × 0.25°, and is available from January 1, 1993 to the present.

The daily sea surface temperature (SST) data at a spatial resolution of 0.05° × 0.05° are generated from satellite and *in situ* observations by Operational Sea Surface Temperature and Sea Ice Analysis (OSTIA) (Good et al., 2020).

The sea surface wind (SSW) data are 10 m wind field from the Cross Calibrated Multi-Platform (CCMP) Version 2.0, which has a horizontal resolution of 0.25° × 0.25° and a time interval of 6 h, were provided by the National Aeronautics and Space Administration (NASA) since 2009 (Atlas et al., 2011).

The near-global ocean mesoscale eddy atmospheric-oceanic-biological interaction observational dataset (GOMED), produced by Dong et al. (2022), was used to provide eddy information in this study. In addition, the monthly DMI and Niño3.4 index data are collected from the Koninklijk Nederlands Meteorologisch Instituut (KNMI) Climate Explorer (Trouet and Van Oldenborgh, 2013).

Reanalysis and hindcast products provided by CMEMS are used to quantify the nutrient budgets during the SSC penetrating front events. The Global Ocean Biogeochemistry Hindcast (GOBH; Product ID: GLOBAL_MULTIYEAR_BGC_001_029) provides daily biogeochemical parameters, i.e., the chlorophyll, nitrate (N_a), phosphate (P_a), silicate (Si_a), dissolved oxygen, and primary production, from January 1, 1993 to the present. The corresponding physical parameters are obtained from the Global Ocean Ensemble Physics Reanalysis (GOEPR; Product ID: GLOBAL_MULTIYEAR_PHY_ENS_001_031), including the sea water potential temperature, salinity, SSH, velocity, and mixed layer thickness. Both the GOBH and GOEPR are daily gridded at a 0.25° × 0.25° horizontal resolution from January 1, 1993 to the present.

Fig. 1 shows the comparison of the simulated SSC in GOBH with the satellite observations in upwelling and non-upwelling seasons. The GOBH model has well reproduced the upwelling-related high SSC along the south coast of Java, and relatively larger SSC values in the south of Lombok Strait, during June–November and December–May,

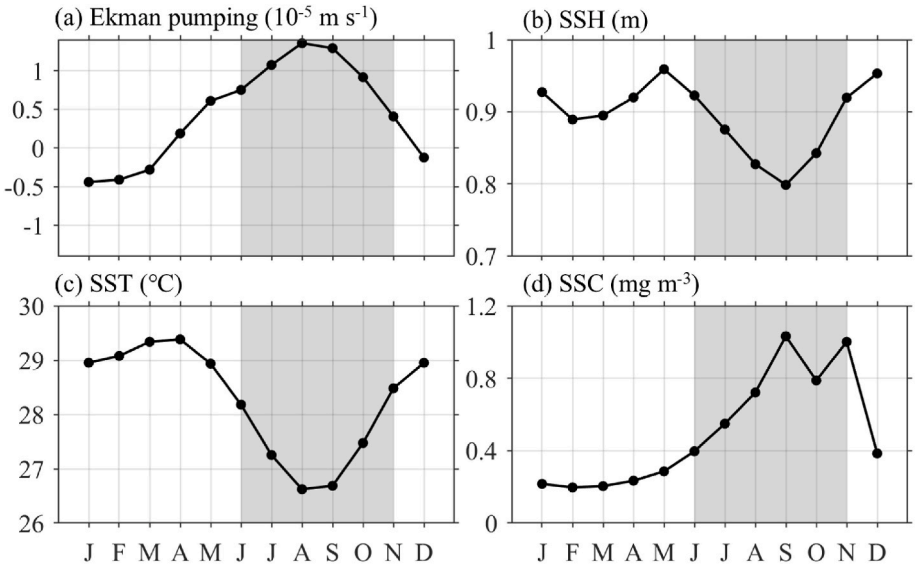

Fig. 2. The area-averaged climatological monthly mean values of (a) Ekman pumping, (b) sea surface height (SSH), (c) sea surface temperature (SST), and (d) SSC in the south of Java Island (area enclosed by blue lines in Fig. 1a) during the period of 1998–2019. The upwelling (June to November) and non-upwelling (December to May) seasons are indicated with gray shadings and without gray shadings, respectively.

respectively. Meanwhile, the widths of high SSC band along the south coast of Java are approximately 100 (50) km in upwelling (non-upwelling) seasons, and were used for the detection of SSC penetrating front as introduced in Section 2.2.

2.2. SSC penetrating front detection

Basically, the SSC penetrating front is identified by detecting the edge of the SSC gradient following Castelao and Wang (2014) and Wang et al. (2020). The mean widths of high SSC band south of Java Island are roughly 100 (50) km during the upwelling (non-upwelling) seasons, resulting in along-shore SSC fronts near the 50–100 km offshore distance isolines. These along-shore SSC fronts are not the penetrating SSC fronts. Therefore, we apply two criteria to exclude these fake penetrating fronts: 1) the coastal regions were masked to exclude along coast fronts induced by coastal currents and upwelling; (2) the detected front pixels should be continuously distributed in the offshore direction. When counting the number of occurrences of SSC penetrating fronts, only those with an offshore direction that penetrate at least 100 (50) km offshore during upwelling (non-upwelling) periods are included.

2.3. Nutrient budget analyses

Based on the GOBH and GOEPR reanalysis data, the mixed layer nutrient budget can be estimated following Moisan and Niiler (1998) and Xu et al. (2024). The variations of the mixed layer nutrients, i.e., nitrate ($\frac{\partial N_a}{\partial t}$), phosphate ($\frac{\partial P_a}{\partial t}$), and silicate ($\frac{\partial Si_a}{\partial t}$) are governed by horizontal advection (*Adv*), vertical entrainment (*Ent*), convergence of shear flow at the mixed layer base (*Con*), vertical and horizontal diffusion (*Vdiff* and *Hdiff*), and biological uptake (*Bio*). Taking N_a as an example, the equations are as follows:

$$\frac{\partial N_a}{\partial t} = Adv + Ent + Con + Vdiff + Hdiff + Bio \tag{1}$$

$$Adv = -\vec{v}_a \cdot \nabla N_a \tag{2}$$

$$Ent = -\frac{1}{h}(N_a - N_{-h}) \times \left(\frac{\partial h}{\partial t} + \vec{v}_{-h}\nabla h + w_{-h}\right) \tag{3}$$

$$Con = -\frac{1}{h}\nabla \cdot \left(\int_{-h}^{0} \vec{v}' N' dz\right) \tag{4}$$

$$Vdiff = \frac{1}{h}\int_{-h}^{0} A_v \frac{\partial^2 N}{\partial z^2} dz \tag{5}$$

$$Hdiff = \frac{1}{h}\int_{-h}^{0} A_h \left(\frac{\partial^2 N}{\partial x^2} + \frac{\partial^2 N}{\partial y^2}\right) dz \tag{6}$$

$$Bio = \frac{1}{h}\nabla \cdot \left(\int_{-h}^{0} Biology_N\right) \tag{7}$$

$$N_{new\_supply} = Adv + Ent + Con + Vdiff + Hdiff \tag{8}$$

where $\vec{v}_a$ and N_a are the vertically averaged velocity and nutrients in the mixed layer with a depth of h; $\vec{v}_{-h}$ and N_{-h} are the velocity and nutrients at the base of the mixed layer; w_{-h} is the entrainment rate estimated as $w_{-h} = -\int_{-h}^{0} \nabla \cdot \vec{v}_a dz$; $\vec{v}'$ and N' are the deviations of the values in the mixed layer from those in the entire water column, i.e., $\vec{v}' = \vec{v} - \vec{v}_a$, and $N' = N - N_a$, with $\vec{v}$ and N denoting the vertically averaged velocity and nutrients over the entire water column; A_v and A_h are the vertical and horizontal diffusivity coefficients, taken as 4×10^{-5} m^2 s^{-1} and 10^3 m^2 s^{-1}, respectively. The biological term (*Bio*) reflects the balance between nutrient uptake by phytoplankton and new nutrient supply by dynamical processes, and thus can be estimated as $Bio = \frac{\partial N_a}{\partial t} - N_{new\_supply}$, where N_{new_supply} is the sum of the first five terms on the right-hand side of Eq. (1).

3. Results

3.1. SSC penetrating fronts in upwelling and non-upwelling seasons

As shown in Fig. 2, in response to the onset of the Southeast Monsoon, the offshore Ekman transport induced by Ekman pumping is upward (>0) from April to November; SSH has double peaks in May and December; SST is generally out of phase with Ekman pumping and in phase with SSH, showing climatological cooling stage from June to October; SSC, which is closely associated with the upward transport of

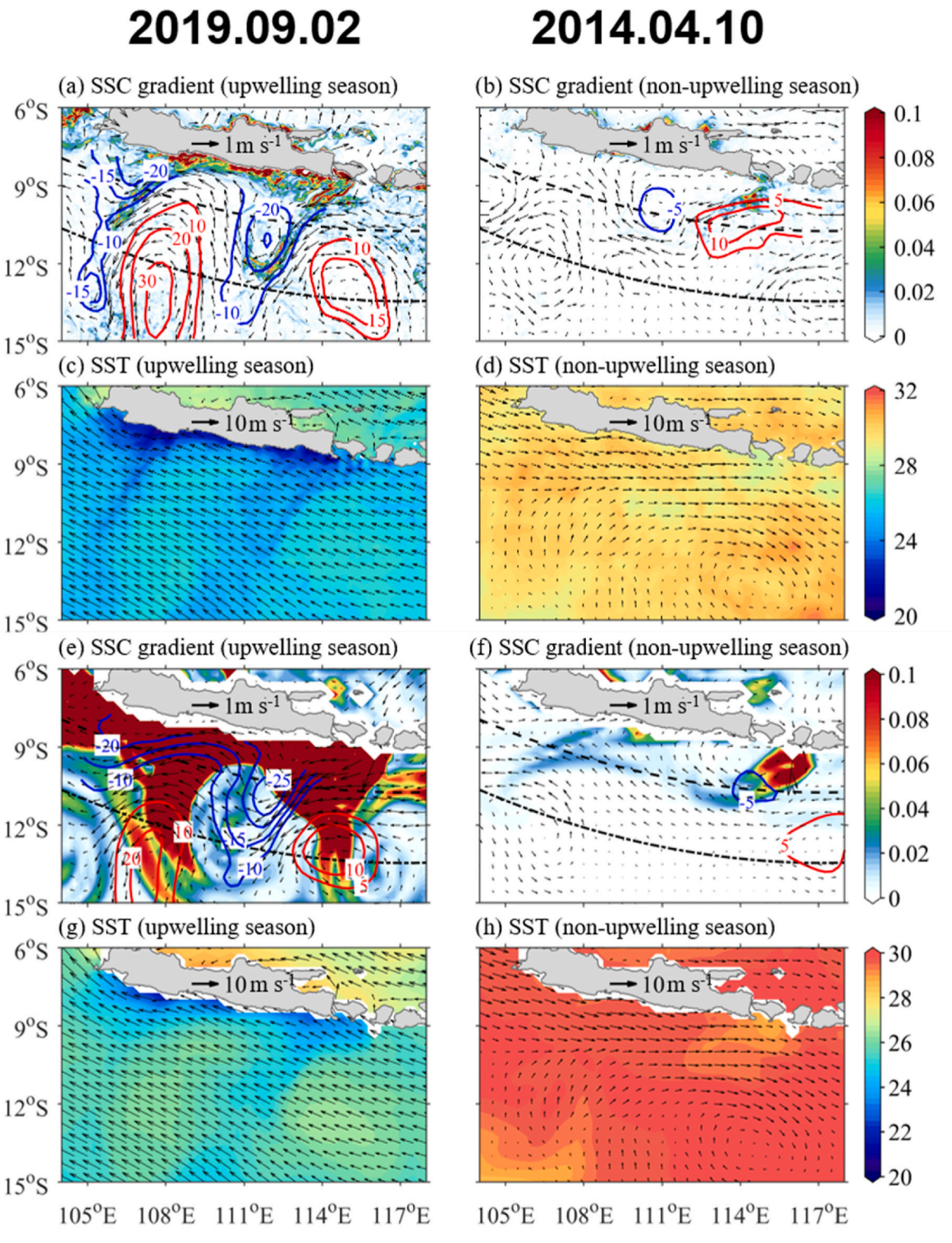

Fig. 3. Typical sea surface chlorophyll-a (SSC) penetrating fronts (identified by SSC gradient, shading, unit: mg m^{-3} km^{-1}) south of the Java Island during (a) upwelling and (b) non-upwelling periods. Red (blue) contours denote the sea surface height anomalies (unit: cm) for anticyclonic (cyclonic) eddies, black dashed (dot) contours indicate offshore distance isolines of 200 (500) km, and vectors represent the sea surface geostrophic currents (unit: m s^{-1}), respectively. The synchronous sea surface temperature (shading, unit: °C) and sea surface wind (vectors, unit: m s^{-1}) are depicted in (c) and (d). Panels (e)–(h) are the same as (a)–(d), but are derived from the Global Ocean Biogeochemistry Hindcast (GOBH) and Global Ocean Ensemble Physics Reanalysis (GOEPR) datasets. (For interpretation of the references to colour in this figure legend, the reader is referred to the Web version of this article.)

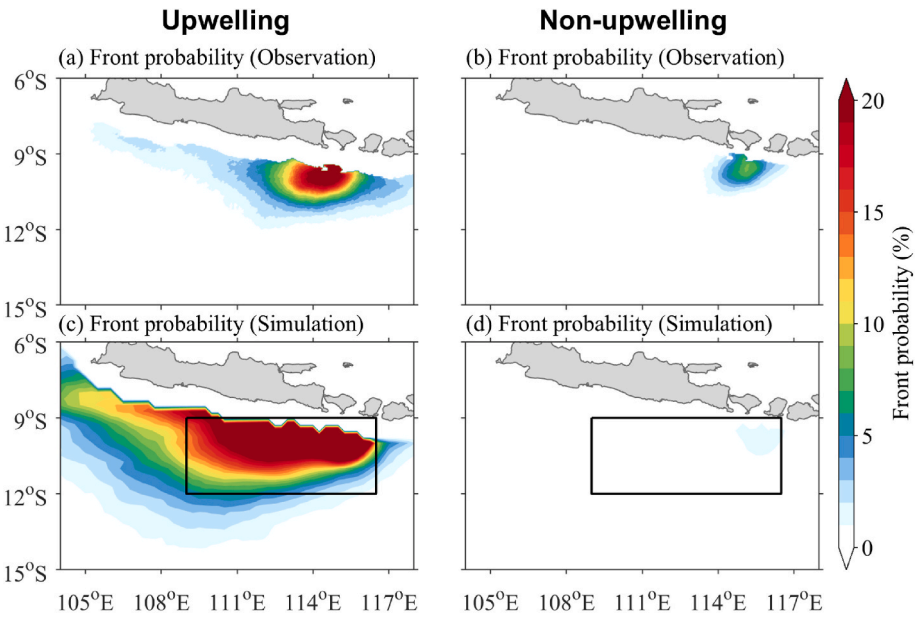

Fig. 4. Monthly mean frontal probability (unit: %) during (a) upwelling (June to November) and (b) non-upwelling (December to May) periods in satellite observations; (c) and (d) are the same as (a) and (b), but from the Global Ocean Biogeochemistry Hindcast (GOBH) dataset. The black boxes in (c) and (d) are defined for conducting nutrient budget analysis in Section 3.3.

nutrients by upwelling, shows a rapid increase since June, reaching and persisting at values greater than 0.8 mg m^{-3} from September throughout November. Therefore, we defined the upwelling (June to November) and non-upwelling (December to May) seasons based on the monsoon-driven Ekman pumping, SSH, SST, and SSC, referring to previous investigations (e.g., Susanto and Marra, 2005; Horii et al., 2020).

The SSC penetrating front off the south Java coast could occur in both the upwelling and non-upwelling seasons (Fig. 3). During the upwelling season, in addition to the strong SSC front along the south Java coast, two southwestward SSC fronts are detected along offshore distance isolines off the southern Java coast. These fronts are located at approximately 440 km offshore from western Java and 480 km offshore west of Lombok Strait, respectively (Fig. 3a). These two SSC penetrating fronts coincide with the edges between a cyclonic eddy and an anticyclonic eddy. During the non-upwelling season, there is only one weak SSC penetrating front south of the Lombok Strait, with an offshore distance of approximately 200 km (Fig. 3b), occurring along the edge between a cyclonic-anticyclonic eddy pair. The penetrating-like fronts could also be revealed by the SST distribution during upwelling season (Fig. 3c). During the non-upwelling season, there is no evidence of a penetrating-like front in the SST distribution (Fig. 3d). Compared to the observation, the SSC penetrating fronts are capable of being reproduced in the GOBH dataset in both upwelling and non-upwelling seasons, albeit with much stronger intensity in SSC gradient, which may be partly attributed to overestimated chlorophyll-a concentration in the model (Fig. 3e–h).

The SSC fronts occur most frequently in the regions southwest of the Lombok Strait in both the upwelling and non-upwelling seasons, with a front probability of up to 60 % and 13 %, respectively (Fig. 4). During the upwelling season (June to November), the fronts occur more than 20 times in July, August and September, and decrease to 14 and 4 in October and November (Fig. 4a). In comparison, there are rarely any penetrating fronts occurring in December to March of the non-upwelling season, attributed to the lack of nutrient supplement (Fig. 4b). The front probability detected from the GOBH modeled data generally shows larger/small values in upwelling/non-upwelling seasons, probably due to the background SSC being strongly associated with seasonal upwelling in the model (Fig. 4c and d). Nevertheless, there are still SSC penetrating fronts occurring in non-upwelling seasons with a probability of approximately 2 %.

3.2. *Nutrient budget analyses for SSC penetrating front events*

Nutrient budget analysis was conducted for the SSC penetrating front events in both upwelling (Fig. 5) and non-upwelling (Fig. 6) seasons. The negative variations suggest consumption of nutrients by phytoplankton in the mixed layer (Fig. 5a–c), which results in an increase in SSC to form the penetrating fronts along the south coast of Java (Fig. 4a and e). During the upwelling season, there is a rich nutrient supply in the mixed layer along the south coast of Java. These nutrients are transported offshore by active mesoscale eddies, as suggested by previous investigations (Yang et al., 2019; Xu et al., 2021), and evidenced by the *Adv* terms of the nutrient budget equation (Fig. 5d–f). The *Ent*, *Con*, *Vdiff* and *Hdiff* terms contribute little to the mixed layer nutrients (Fig. 5g–r). The nutrient budget analysis is in accordance with the background dynamical fields and explains the formation of SSC penetrating front (Fig. 3e and g). In Fig. 3e and g, we can see anticyclonic-cyclonic-anticyclonic eddies from west to east in the southern tropical Indian Ocean. The westward current along the warm eddy largely induces the positive-negative pattern in *Adv* terms south of the central Java Island (Figs. 3e and 5d–f). Meanwhile, the presence of a warm and deep mixed layer hinders the growth of phytoplankton within the anticyclonic eddy; in contrast, a faster growth of phytoplankton is expected within the cyclonic eddy (Fig. 5v–x). As a result, nutrients are accumulated (or consumped) (Fig. 5d–f), and SSC shows a lower-higher distributed in the anticyclonic-cyclonic eddy pair, which in turn gives rise to the formation of SSC penetrating front (Fig. 3e).

During non-upwelling seasons, nutrient levels significantly decrease in the southern tropical Indian Ocean. Specifically, the nutrient variations and new nutrient supply for N_a and P_a are generally one order of magnitude smaller than those in the upwelling season (left and middle subpanels of Fig. 6). It can also be found that the spatial pattern of the new nutrient supply—i.e., for N_a, P_a and Si_a—is different from each other (Fig. 6s–u). Moreover, nutrient consumption by biological uptake is maintained at a low level (Fig. 6v–x). These results indicate that the N_a:P_a ratio is uncoordinated or unbalanced, which is not favorable for the growth of phytoplankton (especially in the southwest of Java Island) (Fig. 6s–x).

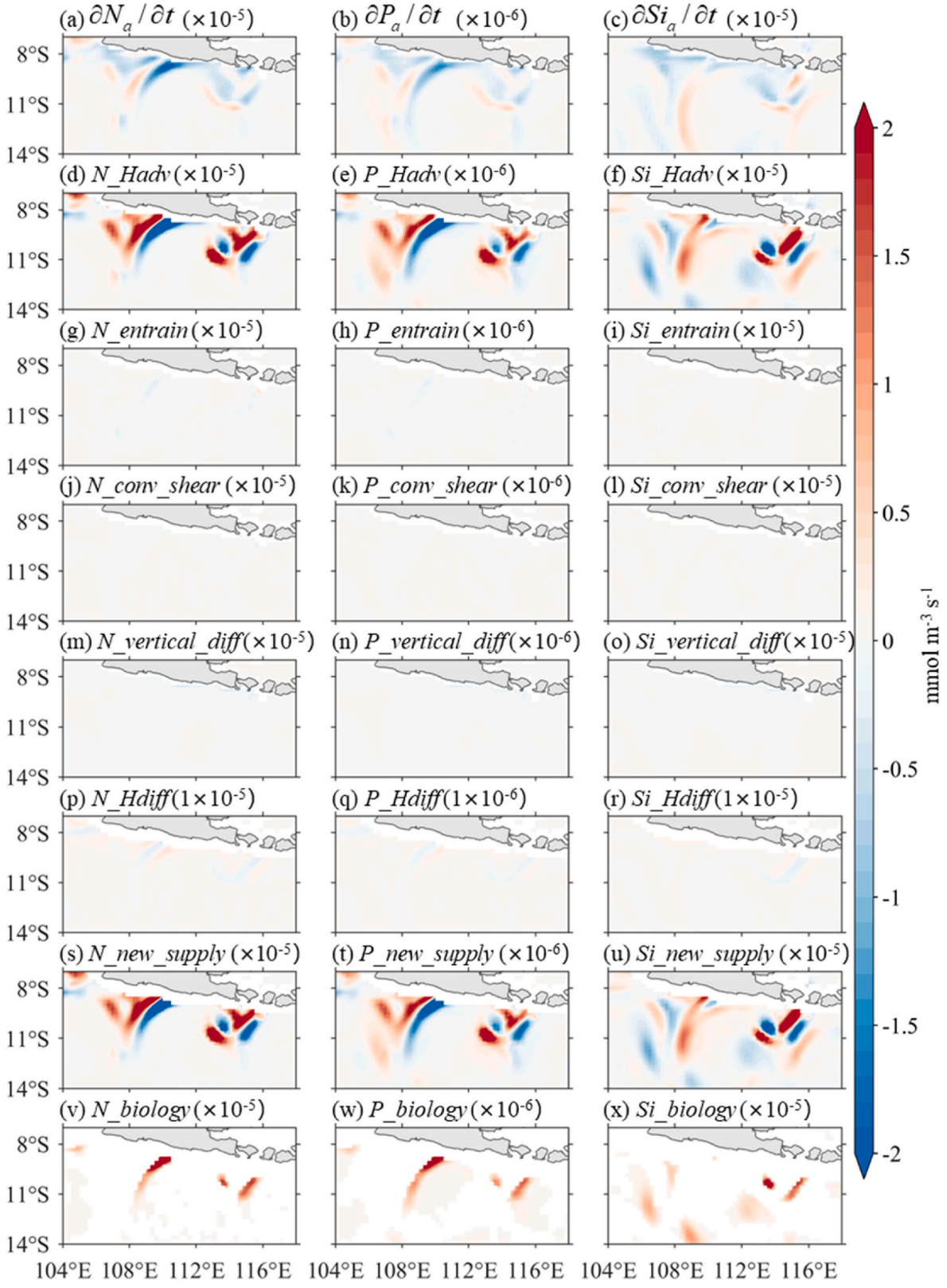

Fig. 5. Mixed layer nutrient budget of nitrate (N_a, left subpanels), phosphate (P_a, middle subpanels), and silicate (Si_a, right subpanels) for the sea surface chlorophyll-a (SSC) penetrating front event on September 2, 2019 (upwelling season). Nutrient variations in (a) N_a, (b) P_a, and (c) Si_a, along with corresponding right-hand terms contributing to the nutrient variations in Eq. (1): (d)–(f) horizontal advection (*Adv*), (g)–(i) vertical entrainment (*Ent*), (j)–(l) convergence of shear flow at the mixed layer base (*Con*), (m)–(o) vertical diffusion (*Vdiff*) and (p)–(r) horizontal diffusion (*Hdiff*), (s)–(u) the total new nutrient supply; and (v)–(x) the biological uptake (*Bio*).

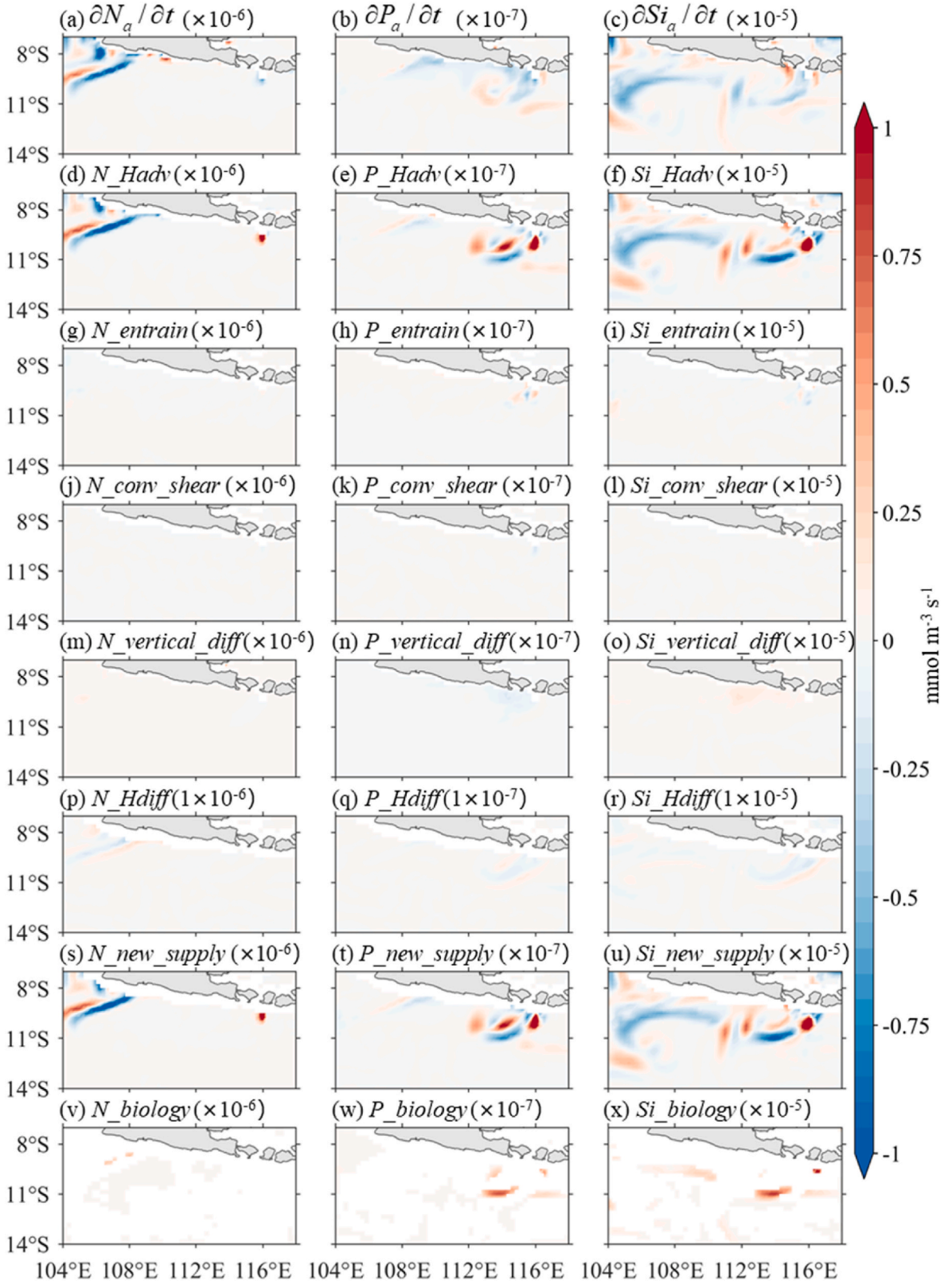

Fig. 6. Same as Fig. 4, but for the case on April 10, 2014 (non-upwelling season).

3.3. Seasonal cycle and interannual variability of the SSC penetrating fronts

During the upwelling season (June to November), the fronts occur more than 20 times with maximum SSC gradients of 0.74, 0.86, and 0.93 mg m^{-3} km^{-1} in July, August and September, and decrease to 14 and 4 times in October and November with maximum SSC gradients of 0.72 and 0.45 mg m^{-3} km^{-1} (Fig. 7a). In comparison, there are rarely any front occurrences from December to March during the non-upwelling season, attributed to the lack of nutrient supplement. The

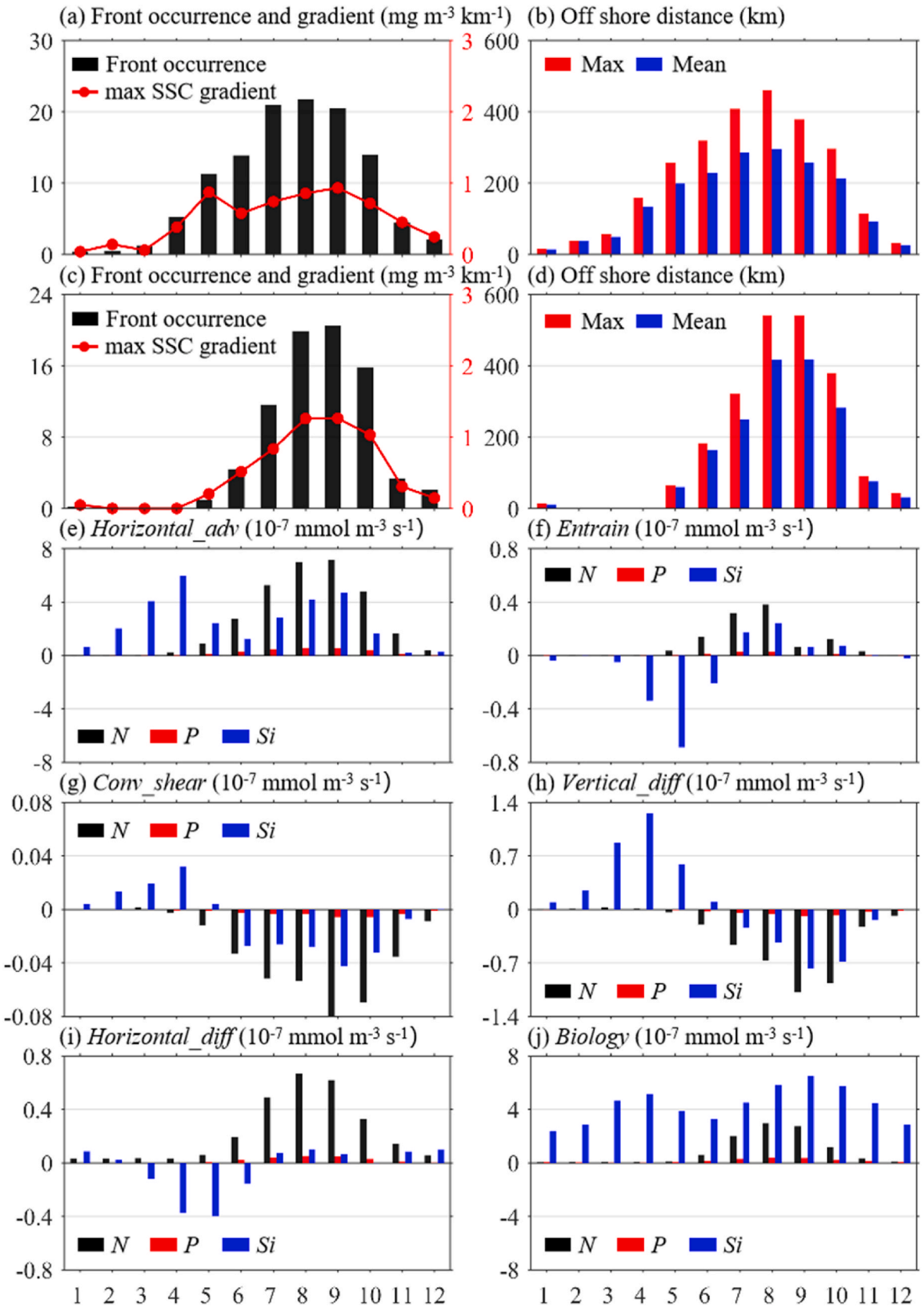

Fig. 7. Climatological monthly mean values of (a) occurrence numbers (black) and maximum SSC gradient (red), and (b) maximum (red) and mean (blue) offshore distance of the SSC penetrating front in the south off the Java Island in satellite observations; (c) and (d) are the same as (a) and (b), but from the Global Ocean Biogeochemistry Hindcast (GOBH) dataset; Right-hand terms contributing to the nutrient variations in Eq. (1): (e) horizontal advection (*Adv*), (f) vertical entrainment (*Ent*), (g) convergence of shear flow at the mixed layer base (*Con*), (h) vertical diffusion (*Vdiff*) and (i) horizontal diffusion (*Hdiff*), (j) the biological uptake (*Bio*), averaged over the black box region in Fig. 4c. (For interpretation of the references to colour in this figure legend, the reader is referred to the Web version of this article.)

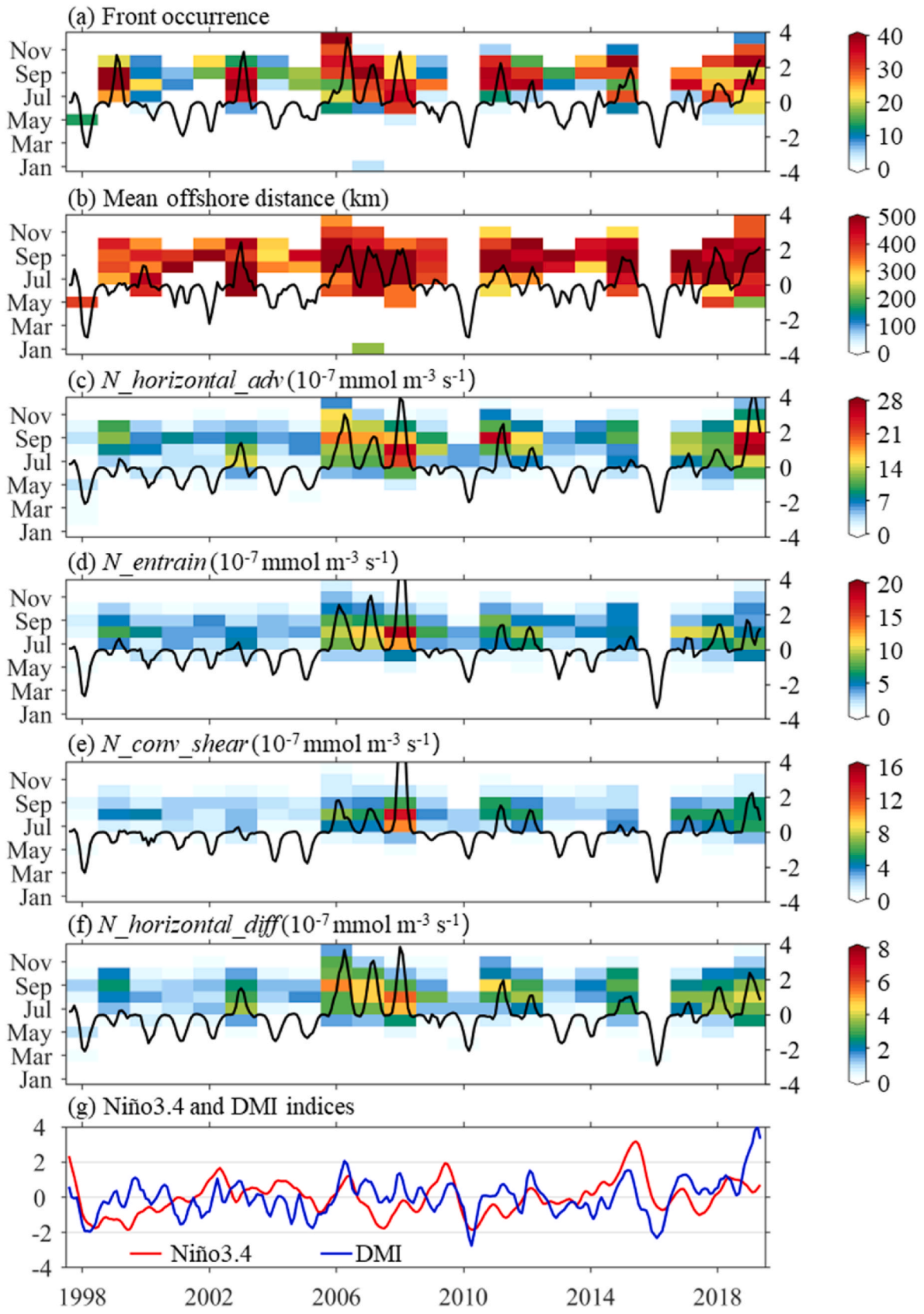

Fig. 8. (a) Monthly mean occurrence values (shading) of the SSC penetrating front south off the Java Island (area-averaged values within the black box in Fig. 4c), and its anomaly (black line) during the period of 1998–2018; (b) the same as (a), but for the mean offshore distance; and corresponding right-hand terms contributing to the nutrient variations in Eq. (1): (c) horizontal advection (*Adv*), (d) vertical entrainment (*Ent*), (e) convergence of shear flow at the mixed layer base (*Con*), and (f) horizontal diffusion (*Hdiff*), respectively; (g) Niño3.4 (red) and DMI (blue) indices. (For interpretation of the references to colour in this figure legend, the reader is referred to the Web version of this article.)

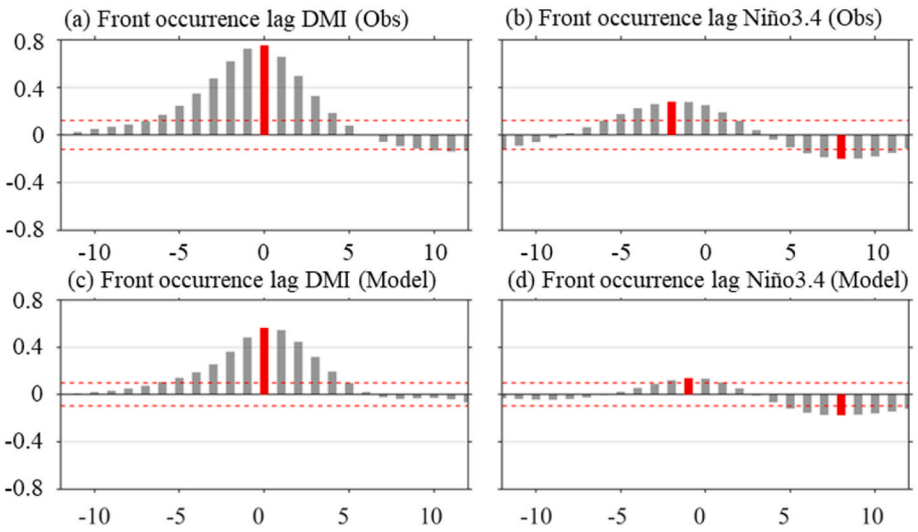

Fig. 9. Lag correlations of SSC penetrating front occurrence anomalies with (a) DMI and (b) Niño3.4 indices in observation; and (c) DMI and (d) Niño3.4 indices in the Global Ocean Biogeochemistry Hindcast (GOBH) dataset. Negative and positive values on the x-axis indicate the lead and lag months of the front occurrence, respectively. Red bars indicate peak values, and the 95 % significance level is marked by the red dashed horizontal lines. (For interpretation of the references to colour in this figure legend, the reader is referred to the Web version of this article.)

front occurrence increases to 5 times with a maximum SSC gradient of 0.38 mg m^{-3} km^{-1} starting from April, and reaches up to 14 times with a maximum SSC gradient of 0.58 mg m^{-3} km^{-1} in June. The maximum (mean) offshore distances of the SSC front increase from 160 (134) km in April to 461 (296) km in August, and then decrease to 115 (92) km in November (Fig. 7b). Basically, the front occurrence and its offshore distance are more frequent/larger in upwelling seasons when there is a shallower thermocline; however, the front occurrence could also reach a climatological mean of 11 and 14 times per month in May and June, before the onset of thermocline shoaling (Figs. 2b and Fig. 7a–b). The modeled occurrence and offshore distance of the SSC penetrating front are basically consistent with the observation, albeit with a lower occurrence frequency than the observation during the non-upwelling season (Fig. 7c–d). The *Adv*, *Ent* and *Hdiff* terms positively contribute to nutrients supply of *N* and *P* during the upwelling season, with Adv as the dominant term, approximately 1.7–7.1 $\times$ 10^{-7} mmol m^{-3} s^{-1}(N_a) and 0.2–4.7 $\times$ 10^{-7} mmol m^{-3} s^{-1} (P_a), accounting for 59.6–70.0 % (N_a) and 43.2–58.2 % (P_a) of the total variations, respectively. The *Con* and *Vdiff* terms negatively contribute to the nutrient supply of N_a and P_a, but the values are only 1/6 of the *Adv* terms (Fig. 7e–i). The growth of phytoplankton is mainly determined by N_a and P_a, as evidenced by the biological uptake of these nutrients (Fig. 7j). The Si_a does not act as a crucial factor for phytoplankton growth, which may be attributed to the fact that the source of Si_a is not in accordance with those of N_a and P_a (Ayers et al., 2014; Talley and Sprintall, 2005).

The SSC penetrating fronts exhibit significant interannual variability, which are more active in 1999, 2002, 2003, 2006, 2007, 2008, 2011, 2012, 2015, 2017, 2018 and 2019. The most active SSC penetrating fronts occur in 2006, with an occurrence of 40.43 $\pm$ 9.55 times and lasting from June to December (Fig. 8a). The interannual variability of the mean offshore distance generally coincides with that of front occurrences (Fig. 8b). Although the *Ent*, *Con*, and *Hdiff* terms contribute an order of magnitude less than the *Adv* term for an individual SSC penetrating front event (Fig. 5), these terms could contribute comparably to the *Adv* terms on the interannual time scale (Fig. 8c–f). As shown in Fig. 8g, the negative SSH anomaly is directly associated with the Indian Ocean Dipole (IOD) event, and the Dipole Mode Index (DMI) time series are out of phase (in phase) with the front occurrences and their mean offshore distance anomalies. In comparison, the front occurrence and its mean offshore distance anomalies show a phase lag of several months relative to the Niño3.4 indices, suggesting a possible impact of the El Niño-Southern Oscillation (ENSO) events (Fig. 8).

The relationship of SSC penetrating front occurrence with IOD and ENSO can be further corroborated by lag correlation analysis (Fig. 9). The results show a maximum positive correlation of 0.76 at 0 time lag between the front occurrence anomalies and DMI indices (Fig. 9a). The correlation coefficients between the front occurrence anomalies and Niño3.4 indices are negatively significant with a time lag of 6–11 months, and peak at an 8-months lag (Fig. 9b). The IOD is strongly influenced by ENSO through teleconnection, i.e., an El Niño event (peaking in boreal winter) tends to trigger a positive IOD event (peaking in the following fall), thereby resulting in a significant negative lag correlation between the DMI and Niño3.4 indices (Stuecker et al., 2017; Xiao et al., 2022). Therefore, the significant negative correlations of front occurrence with Niño3.4 (lagging by 6–11 months) are dominated by the IOD-ENSO relationship. The lag correlations are well reproduced by the GOBH and GBEPR models (Fig. 9c–d), suggesting a reasonable coupling between the dynamical and biochemical processes in the models. Thus, we can further explore the underlying mechanisms through which IOD and ENSO impact the SSC penetrating front.

Fig. 10 presents the composited probability of the SSC penetrating front and the associated nutrient budget for positive and negative Indian Ocean Dipole (IOD) events. The results indicate that more SSC penetrating fronts occur in positive IOD years, both in observations and simulations (Fig. 10a and b). During positive IOD events, the increased occurrences of SSC penetrating fronts are primarily sustained by the nutrients induced by horizontal advection (Fig. 10c). Vertical entrainment and horizontal diffusion play secondary roles in the south of Lombok Strait and along the south coast of Java, respectively, while the convergence of shear flow at the mixed layer base contributes relatively little to the nutrient supply in the mixed layer (Fig. 10d–f).

The occurrence probability of the SSC penetrating front is higher (lower) in El Niño (La Niña) years, but these differences are comparatively smaller than those associated with IOD events (Fig. 11a and b). In terms of the nutrient budget, the nutrient anomalies are mainly induced by the *Adv* (Fig. 11c) and *Hdiff* terms (Fig. 11f). There are no significant differences in the *Ent* and *Con* terms between the El Niño and La Niña events (Fig. 11d–e).

4. Discussion

In the southeastern tropical Indian Ocean along the south coast of

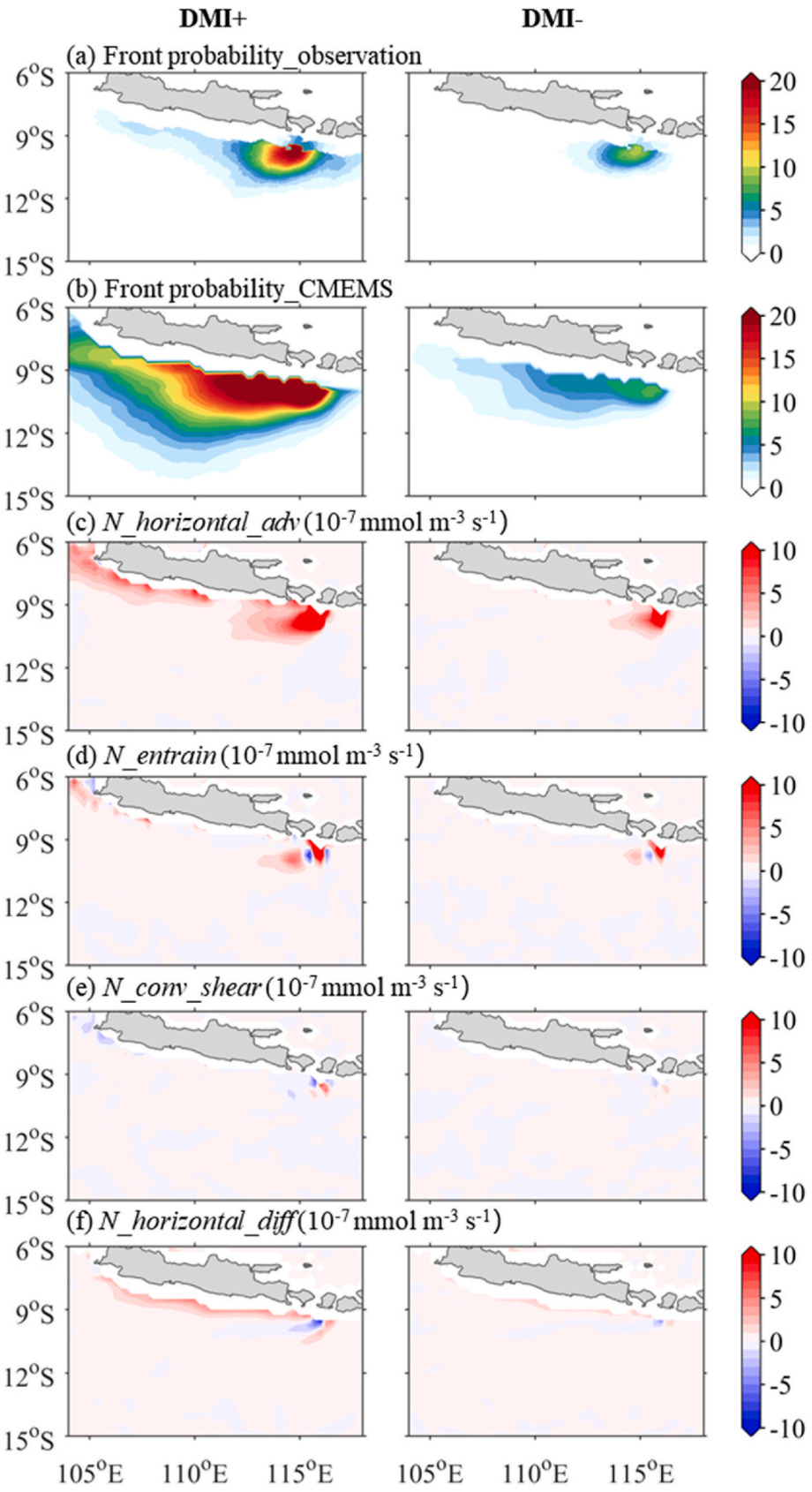

Fig. 10. Composite of (a) SSC penetrating front probability in satellite observations and (b) that from the Global Ocean Biogeochemistry Hindcast (GOBH) dataset; (c) horizontal advection (*Adv*), (d) vertical entrainment (*Ent*), (e) convergence of shear flow at the mixed layer base (*Con*), and (f) horizontal diffusion (*Hdiff*) (terms of nutrient budget) derived from the Global Ocean Ensemble Physics Reanalysis (GOEPR) dataset. The left and right panels are composited from the positive and negative Indian Ocean Dipole (IOD) events, respectively.

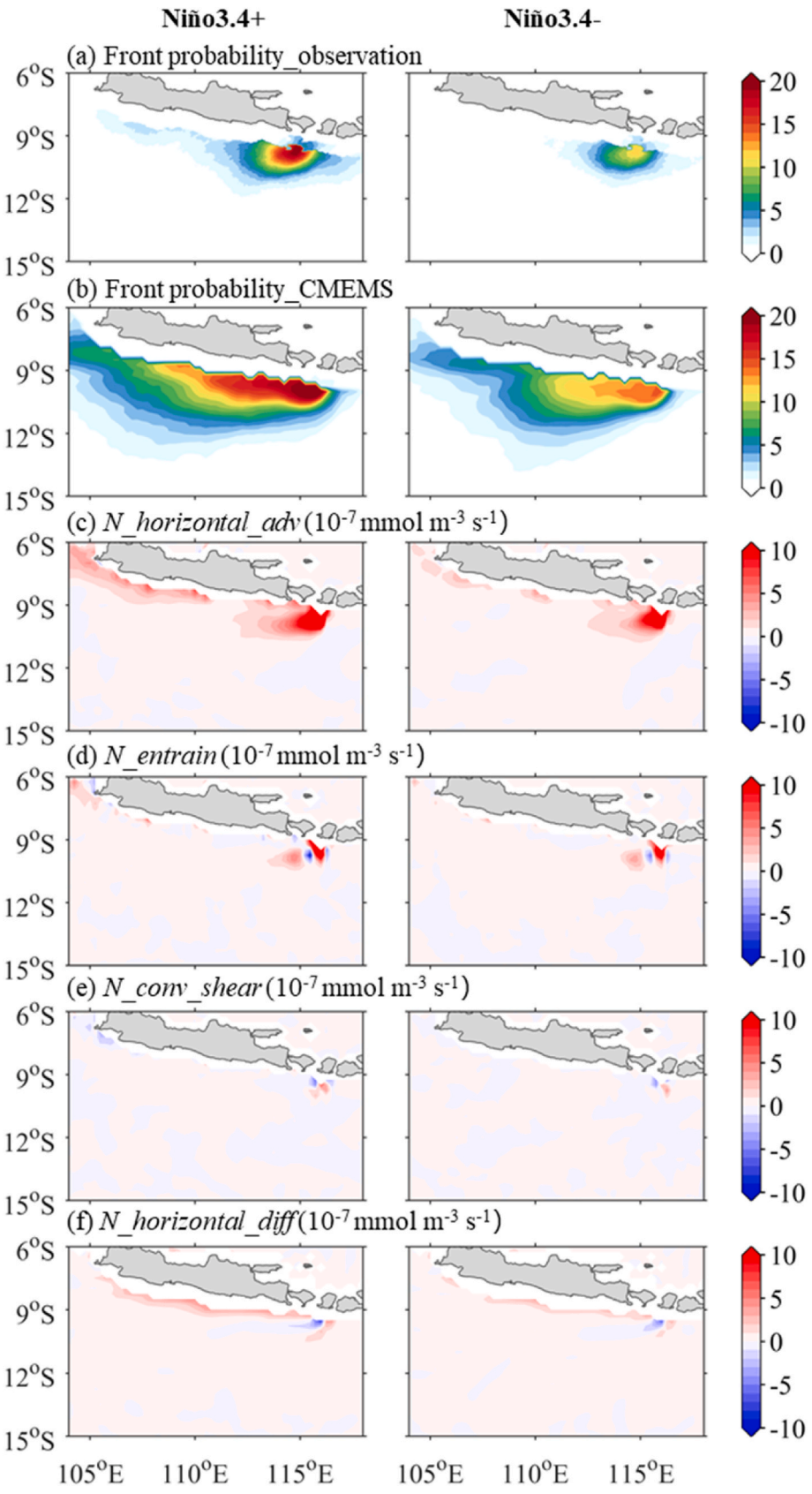

Fig. 11. Same as Fig. 9, but for the El Niño and La Niña conditions.

Java, it is prominently characterized by seasonal upwelling, which plays a crucial role in the seasonal bloom of SSC by carrying nutrient-rich waters from the deeper layer to the mixed layer (Xu et al., 2021). The upwelling, however, is generally confined to a narrow range off the Java coast (Susanto et al., 2001; Horii et al., 2020; Xu et al., 2021), and is not capable of generating long-distance offshore SSC penetrating fronts roughly as far as 500 km (Fig. 3). Yang et al. (2019) reported higher SSC anomalies in cyclonic eddies off the Java coast within 0–400 km, attributed to vertical upwelling within these cyclonic eddies, and horizontal advection of high SSC carried by them. Xu et al. (2021) reported intraseasonal SSC variability induced by the propagation of coastal Kelvin waves (along the south coast of Java) and mesoscale eddies (off the south coast of Java), respectively.

In addition to the increase in SSC induced by the previously mentioned upwelling events and cyclonic eddies, here, we identified the SSC penetrating front south off the Java Island (Fig. 3). This front typically forms along the edge between a cyclonic-anticyclonic eddy pair. It could occur in both upwelling and non-upwelling seasons, with an offshore distance of up to 500 km. Nutrient budget analysis suggests that the SSC penetrating front is related to the horizontal advection of nutrients, which is particularly induced by the jet along the edge between the cyclonic-anticyclonic eddy pair (Fig. 5). The role of mesoscale eddies is corroborated by their seasonal variation, showing relatively weak intensity during the first half of the year and then becoming enhanced with peak intensity in October (Zu et al., 2022). This seasonal variation basically coincides with that of the front occurrence and offshore extension of the SSC penetrating front (Fig. 7). In comparison, there are very few occurrences of the SSC penetrating front during the non-upwelling season, attributed to limited nutrients and an unfavorable N_a:P_a ratio for phytoplankton growth (Figs. 5–7). Therefore, we conclude that the upwelling events provide background nutrient-rich waters along the south coast of Java. Subsequently, horizontal advection induces long-distance offshore transport of nutrients, which in turn favors the formation of the SSC penetrating fronts. During the non-upwelling seasons, the SSC penetrating front could only occur south of the Lombok Strait. This is probably related to the Indonesian Throughflow (ITF), which transports nutrients from the Indonesian seas (Xie et al., 2019, 2024). The N_a:P_a ratio in the Indonesian seas is lower than the Redfield ratio of 16:1 (Redfield, 1958), and thus results in a nitrogen limitation for the growth of phytoplankton in the south of the Lombok Strait (Xie et al., 2019, 2024).

The southeastern tropical Indian Ocean is the key area where the IOD events happen (Saji et al., 1999). During positive IOD events, there are shallower mixed layers and thermoclines, making it easier for the nutrient-rich waters to reach the mixed layer from the deeper layer, enhancing the nutrient supply for phytoplankton growth (Xu et al., 2021). Meanwhile, eddy activity is more energetic during IOD events, favoring long-distance advection by the offshore jets along the edges between cyclonic-anticyclonic eddy pair (Ogata and Masumoto, 2011; Yang et al., 2015; Chen et al., 2020). As a result, SSC penetrating fronts occur more frequently in positive IOD events, with horizontal advection (vertical entrainment) of nutrients acting as the primary (secondary) contributors, respectively (Fig. 10). The occurrences of SSC penetrating fronts are also associated with ENSO events, showing more frequent occurrences during El Niño events with slightly stronger advection. The differences between El Niño and La Niña events, however, are smaller than those between positive and negative IOD events (Fig. 11).

5. Summary

In this study, we have reported the SSC penetrating front phenomenon south of Java Island based on satellite observations. A typical SSC penetrating front tends to occur along the edge between a cyclonic-anticyclonic eddy pair, and could be observed in both upwelling and non-upwelling seasons, with offshore distance of up to 500 km. The SSC penetrating fronts more frequently occur during the upwelling season (July to November), with longer offshore distances. The mechanism is mainly attributed to the adequate supply of nutrients in the upwelling region, and the strong advection induced by offshore jets along the edge between a cyclonic-anticyclonic eddy pair. The SSC penetrating fronts rarely appears due to nutrient scarcity and an unfavorable N_a:P_a ratio; however, the ITF transporting nutrients from the Indonesian seas is an important source for the growth of phytoplankton near the Lombok Strait. The interannual variability of the SSC penetrating fronts is influenced by IOD, rather than ENSO events, since there are shallower mixed layer and thermocline, as well as more active eddies in the southeastern tropical Indian Ocean. Besides seasonal upwelling and mesoscale eddies, submesoscale processes have been revealed to play important roles in the SSC variations (e.g., Lévy et al., 2012; Mahadevan, 2016; Guo et al., 2019; Zhang et al., 2019). However, we did not take these processes into consideration because the model resolution used in this study cannot resolve submesoscale processes. Moreover, *in situ* observations are needed to verify the mechanisms of the SSC penetrating fronts. By employing a high-resolution ocean dynamic model coupled with biogeochemical processes, along with *in situ* observations (e.g., BGC- ARGO, subsurface moorings, buoys, etc), it is expected that we can have a more robust and in-depth recognition of the SSC penetrating fronts off the south coast of Java Island in the future.

CRediT authorship contribution statement

Tengfei Xu: Writing – review & editing, Writing – original draft, Validation, Methodology, Investigation, Formal analysis, Conceptualization. **Dingqi Wang:** Writing – review & editing, Visualization, Software, Methodology, Formal analysis, Data curation. **Qinsheng Wei:** Writing – review & editing, Validation, Investigation, Formal analysis. **Shujiang Li:** Writing – review & editing, Validation, Investigation. **R.D. Susanto:** Writing – review & editing, Investigation. **Guanlin Wang:** Writing – review & editing, Investigation. **Fei Teng:** Writing – review & editing, Visualization, Investigation. **T. Agustiadi:** Writing – review & editing, Investigation. **M. Trenggono:** Writing – review & editing, Investigation. **Priyadi Dwi Santoso:** Writing – review & editing, Investigation. **Zexun Wei:** Writing – review & editing, Validation, Funding acquisition, Conceptualization.

Data availability statement

The data presented in this study are openly and freely available. SSC data are available at https://resources.marine.copernicus.eu/?option=com_csw&view=details&product_id=OCEANCOLOUR_GLO_CHL_L4_REP_OBSERVATIONS_009_082 (accessed on November 30, 2020), WOD2018 data are available at https://www.ncei.noaa.gov/products/world-ocean-database (accessed on November 30, 2020), GHRSST SST data are available at https://podaac.jpl.nasa.gov/dataset/UKMO-L4HRfnd-GLOB-OSTIA (accessed on November 30, 2020), AVISO SSH and sea surface geostrophic currents data are available at http://www.aviso.altimetry.fr/duacs(accessed on November 30, 2020), CCMP wind data are available at http://www.remss.com/measurements/ccmp (accessed on November 30, 2020).

Declaration of competing interest

The authors declare the following financial interests/personal relationships which may be considered as potential competing interests: Zexun Wei reports financial support was provided by Laoshan Laboratory. Zwxun Wei reports financial support was provided by National Natural Science Foundation of China. Tengfei Xu reports financial support was provided by National Natural Science Foundation of China. If there are other authors, they declare that they have no known competing financial interests or personal relationships that could have appeared to influence the work reported in this paper.

Acknowledgments

This study was jointly supported by the National Natural Science Foundation of China (42430402), the Basic Scientific Fund for National Public Research Institutes of China (2024Q02), the Laoshan Laboratory (No. LSKJ202202700), and the Global Change and Air–Sea Interaction II (Contact No. GASI-01-AIP-STwin). Zexun Wei is supported by the Taishan Scholar Program (No. tstp20221148); R. D. Susanto is supported by the Physical Oceanography program of the National Science Foundation (NSF; grant #2242151) through the University of Maryland.

Data availability

Data will be made available on request.

References

Atlas, R., Hoffman, R.N., Ardizzone, J., Leidner, S.M., Jusem, J.C., Smith, D.K., Gombos, D., 2011. A cross-calibrated, multiplatform ocean surface wind velocity product for meteorological and oceanographic applications. Bull. Am. Meteorol. Soc. 92 (1), 2. https://doi.org/10.1175/2010BAMS2946.

Ayers, J.M., Strutton, P.G., Coles, V.J., Hood, R.R., Matear, R.J., 2014. Indonesian throughflow nutrient fluxes and their potential impact on Indian Ocean productivity. Geophys. Res. Lett. 41, 5060–5067. https://doi.org/10.1002/2014GL060593.

Azis Ismail, M.F., Ribbe, J., Arifin, T., Taofiqurohman, A., Anggoro, D., 2021. A census of eddies in the tropical eastern boundary of the Indian Ocean. J. Geophys. Res. Oceans 126, e2021JC017204. https://doi.org/10.1029/2021JC017204.

Carr, M., Friedrichs, M., Schmeltz, M., Noguchi, A., Antoine, D., Arrigo, K., Asanuma, I., Aumont, O., Barber, R., Behrenfeld, M., 2006. A comparison of global estimates of marine primary production from ocean color. Deep Sea Res. Part II Top. Stud. Oceanogr. 53, 741–770. https://doi.org/10.1016/j.dsr2.2006.01.028.

Castelao, R.M., Wang, Y., 2014. Wind-driven variability in sea surface temperature front distribution in the California current system. J. Geophys. Res. Oceans 119, 1861–1875. https://doi.org/10.1002/2013JC009531.

Dong, C., Liu, L.X., Nencioli, F., Benthel, B.J., Liu, Y., Xu, G., Ma, J., Ji, J., Sun, W., Shan, H., Lin, X., Zhou, B., 2022. The near-global ocean mesoscale eddy atmospheric-oceanic-biological interaction observational dataset. Sci. Data 9, 436. https://doi.org/10.1038/s41597-022-01550-9.

Du, Y., Zhang, J., Wei, Z., Yin, W., Wu, H., Yuan, Y., Wang, Y., 2022. Spatio-temporal variability of suspended sediment fronts (SSFs) on the inner shelf of the East China Sea: the contribution of multiple factors. J. Geophys. Res. Oceans 127, e2021JC018392. https://doi.org/10.1029/2021JC018392.

Guo, M., Xiu, P., Chai, F., Xue, H., 2019. Mesoscale and submesoscale contributions to high sea surface chlorophyll in subtropical gyres. Geophys. Res. Lett. 46, 13217–13226. https://doi.org/10.1029/2019GL085278.

He, L., Li, Y., Zhou, H., Yuan, D., 2010. Variability of cross-shelf penetrating fronts in the East China Sea. Deep Sea Res. Part II Top. Stud. Oceanogr. 57, 1820–1826. https://doi.org/10.1016/j.dsr2.2010.04.008.

Hickox, R., Belkin, I., Cornillon, P., Shan, Z., 2000. Climatology and seasonal variability of ocean fronts in the east China, yellow and bohai seas from satellite SST data. Geophys. Res. Lett. 27, 2945–2948. https://doi.org/10.1029/1999GL011223.

Hood, R.R., Beckley, L.E., Wiggert, J.D., 2017. Biogeochemical and ecological impacts of boundary currents in the Indian Ocean. Prog. Oceanogr. 156, 290–325. https://doi.org/10.1016/j.pocean.2017.04.011.

Horii, T., Ueki, I., Ando, K., 2020. Coastal upwelling events, salinity stratification, and barrier layer observed along the southwestern Coast of Sumatra. J. Geophys. Res. Oceans 125, e2020JC016287. https://doi.org/10.1029/2020JC016287.

Iskandar, I., Sasaki, H., Sasai, Y., Masumoto, Y., Mizuno, K., 2010. A numerical investigation of eddy-induced chlorophyll bloom in the southeastern tropical Indian Ocean during Indian Ocean Dipole—2006. Ocean Dyn. 60, 731–742. https://doi.org/10.1007/s10236-010-0290-6.

Kong, F., Dong, Q., Xiang, K., Yin, Z., Li, Y., Liu, J., 2019. Spatiotemporal variability of remote sensing ocean net primary production and major forcing factors in the tropical eastern Indian and western Pacific Ocean. Remote Sens. 11, 391. https://doi.org/10.3390/rs11040391.

Lahlali, H., Wirasatriya, A., Gensac, E., Helmi, M., Kunarso, Kismawardhani, R.A., 2018. Environmental aspects of tuna catches in the Indian Ocean, southern Coast of java, based on satellite measurements. In: Proceedings of the 2018 4th International Symposium on Geoinformatics (ISyG), Malang, Indonesia. https://doi.org/10.1109/ISYG.2018.8612020.

Lévy, M., Ferrari, R., Franks, P.J.S., Martin, A.P., Rivière, P., 2012. Bringing physics to life at the submesoscale. Geophys. Res. Lett. 39, L14602. https://doi.org/10.1029/2012GL052756.

Li, C., Nelson, J.R., Koziana, J.V., 2003. Cross-shelf passage of coastal water transport at the South Atlantic bight observed with MODIS ocean color/SST. Geophys. Res. Lett. 30 (5), 1257. https://doi.org/10.1029/2002GL016496.

Li, Y., Guo, Y., Zhu, Y., Kido, S., Zhang, L., Wang, F., 2022. Variability of heat content and eddy kinetic energy in the sutheast Indian Ocean: roles of the Indonesian throughflow and local wind forcing. J. Phys. Oceanogr. 52, 2789–2806. https://doi.org/10.1175/JPO-D-22-0051.1.

Lumban-Gaol, J., Leben, R.R., Vignudelli, S., Mahapatra, K., Okada, Y., Nababan, B., Mei-Ling, M., Amri, K., Arhatin, R.E., Syahdan, M., 2015. Variability of satellite-derived sea surface height anomaly, and its relationship with bigeye tuna (Thunnus obesus) catch in the eastern Indian Ocean. Eur. J. Remote Sens. 48, 465–477.

Mahadevan, A., 2016. The impact of submesoscale physics on primary productivity of plankton. Annu. Rev. of Mar. Sci. 8, 161–184. https://doi.org/10.1146/annurev-marine-010814-015912.

Malan, N., Archer, M., Roughan, M., Cetina-Heredia, P., Hemming, M., Rocha, C., Schaeffer, A., Suthers, I., Queiroz, E., 2020. Eddy-driven cross-shelf transport in the east Australian current separation zone. J. Geophys. Res. Oceans 125, e2019JC015613. https://doi.org/10.1029/2019JC015613.

Moisan, J.R., Niiler, P.P., 1998. The seasonal heat budget of the north pacific: net heat flux and heat storage rates (1950–1990). J. Phys. Oceanogr. 28 (3), 401–421. https://journals.ametsoc.org/view/journals/phoc/28/3/1520-0485_1998_028_0401_tshbot_2.0.co_2.xml.

Ogata, T., Masumoto, Y., 2011. Interannual modulation and its dynamics of the mesoscale eddy variability in the southeastern tropical Indian Ocean. J. Geophys. Res. Oceans 116, C05005. https://doi.org/10.1029/2010JC006490.

Redfield, A.C., 1958. The biological control of chemical factors in the environment. Am. Sci. 46 (3), 205–221.

Ren, J., Xuan, J., Wang, Z., Huang, D., Zhang, J., 2015. Cross-shelf transport of terrestrial Al enhanced by the transition of northeasterly to southwesterly monsoon wind over the East China Sea. J. Geophys. Res. Oceans 120, 5054–5073. https://doi.org/10.1002/2014JC010655.

Saji, N.H., Goswami, B.N., Vinayachandran, P.N., Yamagata, T., 1999. A dipole mode in the tropical Indian Ocean. Nature 401, 360–363. https://doi.org/10.1038/43854.

Setiawan, R.Y., Setyobudi, E., Wirasatriya, A., Muttaqin, A.S., Maslukah, L., 2019. The influence of seasonal and interannual variability on surface chlorophyll-a off the western Lesser Sunda Islands. IEEE J. Sel. Top. Appl. Earth Obs. Rem. Sens. 12, 4191–4197. https://doi.org/10.1109/JSTARS.2019.2948385.

Siswanto, E., Horii, T., Iskandar, I., Gaol, J.L., Setiawan, R.Y., Susanto, R.D., 2020. Impacts of climate changes on the phytoplankton biomass of the Indonesian Maritime continent. J. Mar. Syst. 212, 103451. https://doi.org/10.1016/j.jmarsys.2020.103451.

Stuecker, M.F., Timmermann, A., Jin, F.-F., Chikamoto, Y., Zhang, W., Wittenberg, A.T., Widiasih, E., Zhao, S., 2017. Revisiting ENSO/indian ocean dipole phase relationships. Geophys. Res. Lett. 44, 2481–2492. https://doi.org/10.1002/2016GL072308.

Susanto, R.D., Gordon, A.L., Zheng, Q., 2001. Upwelling along the coasts of java and Sumatra sand its relation to ENSO. Geophys. Res. Lett. 28, 1599–1602. https://doi.org/10.1029/2000GL011844.

Susanto, R.D., Marra, J., 2005. Eff ect of the 1997/98 El niño on chlorophyll a variability along the southern coasts of java and Sumatra. Oceanography (Wash. D. C.) 18 (4), 124–127.

Susanto, R.D., Moore, T.S., Marra, J., 2006. Ocean color variability and Indonesian seas during the SeaWiFS era. G-cubed 7 (5). https://doi.org/10.1029/2005GC001009.

Syamsuddin, M., Saitoh, S.I., Hirawake, T., Syamsudin, F., Zainuddin, M., 2016. Interannual variation of bigeye tuna (Thunnus obesus) hotspots in the eastern Indian Ocean off java. Int. J. Rem. Sens. 37, 2087–2100. https://doi.org/10.1080/01431161.2015.1136451.

Taboada, F.G., Barton, A.D., Stock, C.A., Dunne, J., John, J.G., 2019. Seasonal to interannual predictability of oceanic net primary production inferred from satellite observations. Prog. Oceanogr. 170, 28–39. https://doi.org/10.1016/j.pocean.2018.10.010.

Talley, L.D., Sprintall, J., 2005. Deep expression of the Indonesian throughflow: indonesian intermediate water in the south equatorial current. J. Geophys. Res. Oceans 110, C10009. https://doi.org/10.1029/2004JC002826.

Trouet, V., Van Oldenborgh, G.J., 2013. KNMI climate explorer: a web-based research tool for high-resolution paleoclimatology. Tree-Ring Res. 69 (1.3), 3–13. https://doi.org/10.3959/1536-1098-69.

Wang, X., Cheng, X., Liu, X., Chen, D., 2021. Dynamics of eddy generation in the southeast tropical Indian Ocean. J. Geophys. Res. Oceans 126, e2020JC016858. https://doi.org/10.1029/2020JC016858.

Wang, Y., Yu, Y., Zhang, Y., Zhang, H.R., Chai, F., 2020. Distribution and variability of sea surface temperature fronts in the South China Sea. Estuar. Coast Shelf Sci. 240, 106793. https://doi.org/10.1016/j.ecss.2020.106793.

Wei, X., Liao, X., Zhan, H., Liu, H., 2012. Estimates of potential new production in the Java-Sumatra upwelling system. Chin. J. Oceanol. Limnol. 30, 1063–1067. https://doi.org/10.1007/s00343-012-1281-x.

Wirasatriya, A., Setiawan, J.D., Sugianto, D.N., Rosyadi, I.A., Haryadi, H., Winarso, G., Setiawan, R.Y., Susanto, R.D., 2020. Ekman dynamics variability along the southern coast of Java revealed by satellite data. Int. J. Rem. Sens. 41, 8475–8496. https://doi.org/10.1080/01431161.2020.1797215.

Wu, H., 2015. Cross-shelf penetrating fronts: a response of buoyant coastal water to ambient pycnocline undulation. J. Geophys. Res. Oceans 120, 5101–5119. https://doi.org/10.1002/2014JC010686.

Xiao, H., Lo, M., Yu, J., 2022. The increased frequency of combined El Niño and positive IOD events since 1965s and its impacts on maritime continent hydroclimates. Sci. Rep. 12, 7532. https://doi.org/10.1038/s41598-022-11663-1.

Xie, T., Newton, R., Schlosser, P., Du, C., Dai, M., 2019. Long-term mean mass, heat and nutrient flux through the Indonesian seas, based on the tritium inventory in the Pacific and Indian oceans. J. Geophys. Res. Oceans 124, 3859–3875. https://doi.org/10.1029/2018JC014863.

Xie, T., Cao, Z., Hamzah, F., Schlosser, P., Dai, M., 2024. Nutrient vertical flux in the Indonesian seas as constrained by non-atmospheric helium-3. Geophys. Res. Lett. 51, e2024GL111420. https://doi.org/10.1029/2024GL111420.

Xu, T., Li, S., Hamzah, F., Setiawan, A., Susanto, R.D., Cao, G., Wei, Z., 2018. Intraseasonal flow and its impact on the chlorophyll-a concentration in the sunda strait and its vicinity. Deep sea res. Part I oceanogra. Res. Papers 136, 84–90. https://doi.org/10.1016/j.dsr.2018.04.003.

Xu, T., Wei, Z., Li, S., Susanto, R.D., Radiarta, N., Yuan, C., Setiawan, A., Kuswardani, A., Agustiadi, T., Trenggono, M., 2021. Satellite-observed multi-scale variability of sea surface chlorophyll-a concentration along the south coast of the Sumatra-Java Islands. Remote Sens. 13, 2817. https://doi.org/10.3390/rs13142817.

Xu, Y., Wu, Y., Zhang, J., 2024. The role of subsurface instabilities for increasing chlorophyll concentrations in a warming southern Indian ocean. Deep Sea Res. Part II Top. Stud. Oceanogr. 213, 105355. https://doi.org/10.1016/j.dsr2.2023.105355.

Xuan, J., Huang, D., Pohlmann, T., Su, J., Mayer, B., Ding, R., Zhou, F., 2017. Synoptic fluctuation of the Taiwan warm current in winter on the East China Sea shelf. Ocean Sci. 13, 105–122. https://doi.org/10.5194/os-13-105-2017.

Yang, G., Yu, W., Yuan, Y., Zhao, X., Wang, F., Chen, G., Liu, L., Duan, Y., 2015. Characteristics, vertical structures, and heat/salt transports of mesoscale eddies in the southeastern tropical Indian Ocean. J. Geophys. Res. Oceans 120 (10), 6733–6750. https://doi.org/10.1002/2015jc011130.

Yang, G., Zhao, X., Li, Y., Liu, L., Wang, F., Yu, W., 2019. Chlorophyll variability induced by mesoscale eddies in the southeastern tropical Indian Ocean. J. Mar. Syst. 199, 103209. https://doi.org/10.1016/j.jmarsys.2019.103209.

Ye, P., Xuan, J., Huang, D., 2022. Evolution and dynamics of a summertime penetrating front off the Zhejiang-Fujian coast, China. Sci. China Earth Sci. 65 (3), 556–569. https://doi.org/10.1007/s11430-021-9853-x.

Yuan, D., Li, Y., He, L., Zhou, H., Li, R., Wang, F., Lei, H., Hu, D., 2010. An observation of the three-dimensional structure of a cross-shelf penetrating front off the changjiang mouth. Deep Sea Res. Part II Top. Stud. Oceanogr. 57, 1827–1834. https://doi.org/10.1016/j.dsr2.2010.04.009.

Yuan, D., Qiao, F., Su, J., 2005. Cross-shelf penetrating fronts off the southeast coast of China observed by MODIS. Geophys. Res. Lett. 32, L19603. https://doi.org/10.1029/2005GL023815.

Zhang, Z., Qiu, B., Klein, P., Travis, S., 2019. The influence of geostrophic strain on oceanic ageostrophic motion and surface chlorophyll. Nat. Commun. 10 (1), 2838. https://doi.org/10.1038/s41467-019-10883-w.

Zu, Y., Fang, Y., Sun, S., Yang, G., Gao, L., Duan, Y., 2022. The seasonality of mesoscale eddy intensity in the southeastern tropical Indian Ocean. Front. Mar. Sci. 9, 855832. https://doi.org/10.3389/fmars.2022.855832.